

Heterogeneity of solid neutron-star matter: transport coefficients and neutrino emissivity

P. B. Jones*

Department of Physics, Denys Wilkinson Building, University of Oxford, Keble Road, Oxford, OX1 3RH, UK

ABSTRACT

Calculations of weak-interaction transition rates and of nuclear formation enthalpies show that in isolated neutron stars, the solid phase, above the neutron-drip threshold, is amorphous and heterogeneous in nuclear charge. The neutrino emissivities obtained are very dependent on the effects of proton shell structure but may be several orders of magnitude larger than the electron bremsstrahlung neutrino-pair emissivity at temperatures $\sim 10^9$ K. In this phase, electrical and thermal conductivities are much smaller than for a homogeneous *bcc* lattice. In particular, the reduced electrical conductivity, which is also temperature-independent, must have significant consequences for the evolution of high-multipole magnetic fields in neutron stars.

Key words: dense matter - stars: neutron - pulsars: general.

1 INTRODUCTION

The very extensive pulsar and X-ray source observations now being made require, for their interpretation, an understanding of the condensed-matter physics of neutron-star solid phases. The radiative opacity of a very thin surface layer of depth $\sim 10^3$ cm and matter density $\rho \lesssim 10^7$ g cm $^{-3}$ largely determines the temperature difference between the surface and the interior of the star (see Potekhin, Chabrier & Yakovlev 1997, also Potekhin & Yakovlev 2001, for recent calculations and reviews of earlier work). Atoms in the higher-density part of this layer are completely ionized but the electron Fermi momentum is less than or of the order of 1 MeV/c. The whole layer contains no more than $10^{-10}M_\odot$ and has physical properties which are important only with respect to its radiative opacity and, possibly, in connexion with the composition of the neutron-star atmosphere. In the next layer, with matter densities up to the neutron-drip threshold $\rho_{nd} = 4.3 \times 10^{11}$ g cm $^{-3}$, depth $\sim 10^4$ cm and mass $\sim 10^{-5}M_\odot$, the electrons form a relativistic Fermi gas whose transport coefficients (electrical and thermal conductivities σ and κ) are dependent on the nuclear composition and degree of order of the solid. This is also true of the neutron-drip region with densities above ρ_{nd} which occupies most of the crust volume (depth $\sim 10^5$ cm and mass $\sim 10^{-2}M_\odot$). The fraction of the stellar volume concerned here is so large that its electrical conductivity must be relevant to the evolution of high-multipole components of the magnetic field. Pinning of superfluid neutron vortices by nuclei in this region is believed to be the origin of pulsar glitch phenomena (Ander-

son & Itoh 1975; Ruderman 1976). The neutron-drip region contributes almost all the mechanical rigidity of the crust and its failure under Maxwell or other stresses is assumed to be involved in a number of X-ray emission phenomena, for example, the soft gamma repeaters (SGR; Thompson & Duncan 1995, 1996) and the persistent emission of the anomalous X-ray pulsars (AXP; Thompson et al 2000).

The canonical picture of the solid, both above and below ρ_{nd} , in a neutron star that has not been subject to a long period of accretion since formation, is of a homogeneous *bcc* lattice of even-*Z* nuclei, locally in complete weak-interaction equilibrium. Certainly above, and possibly immediately below, ρ_{nd} , the nuclei are those with closed proton shells. The equation of state below ρ_{nd} has been derived by extrapolations of nuclear parameters from experimentally accessible regions of neutron excess (see Haensel & Pichon 1994 who also summarize earlier work). Pethick & Ravenhall (1995) give a general review of solid phase properties and observe that, above ρ_{nd} , there have been two distinct approaches to the problem of deriving the equation of state. Microscopic calculations of the single-particle states for neutrons and protons inside a Wigner-Seitz cell were described in the classic paper of Negele & Vautherin (1973) and give a complete description of the system apart from the superfluid energy gap. But this approach has not been followed by later workers who have adopted a compressible liquid-drop model (CLDM) with various Skyrme pseudopotentials (Lattimer et al 1985, Douchin & Haensel 2001). Although the CLDM nuclear charge is a continuous variable, the existence of shell effects and of proton pairing require that the crust be composed of successive homogeneous layers of even-*Z* nuclei. In fact, weak-interaction equilibrium cannot be exact owing to

* E-mail: p.jones1@physics.ox.ac.uk

the rapid decrease of weak transition rates as the star cools, which is caused by the potential barrier present in those transitions to odd- Z nuclei. Flowers & Ruderman (1977) noted that, in consequence, at least a small fractional concentration of nuclei with charge deviation $\Delta Z = \pm 2$ from the homogeneous lattice must be present in metastable equilibrium as point defects. But it has been usual to assume that the value of the impurity parameter,

$$Q = \sum_i a_i (Z_i - \bar{Z})^2, \quad (1)$$

defined for a distribution of nuclear charges Z_i with fractional concentrations a_i and mean \bar{Z} , is, in most contexts, negligibly small (several orders of magnitude less than unity).

The extent of heterogeneity in Z at densities $\rho < \rho_{nd}$ has been investigated by several authors. Jog & Smith (1982) and De Blasio (2000) have examined the structure of the interface between successive homogeneous layers. The nature of the constraints under which equilibrium is defined was considered by Jones (1988) who concluded that a distribution in Z must be a feature of the state reached as the star cools. More recently, calculations of the point defect concentration have been made by De Blasio & Lazzari (1998).

Formation enthalpies were calculated by Jones (1999a, 2001) for a number of point-defects in solid neutron-star matter at densities $\rho > \rho_{nd}$. The enthalpies obtained were small and it was argued that an amorphous heterogeneous solid phase must be formed and should persist as the star cools, the melting transition being replaced by a glass transition temperature region.

The conclusion that heterogeneity in Z exists both below and above ρ_{nd} does not seem to have been widely accepted. Undoubtedly, the assumption of a *bcc* lattice, homogeneous in Z , is attractive because it can be simply stated and provides a clear basis for calculations, such as those of transport coefficients. It is also the case that arguments about the role of proton shell-structure and the approach to weak-interaction equilibrium were made only qualitatively by Jones (2001, hereafter Paper I) and were not supported by detailed calculation. Nonetheless, even though amorphous heterogeneous structures are unattractive owing to their greater complexity, if they represent physical reality, it is necessary to consider their effect on the stress-response of the solid and to define as well as possible the consequent degree of uncertainty in calculations of transport coefficients and neutrino emissivities. The present paper contains the results of those detailed calculations which were absent from the previous papers. In Section 2, we consider how the effects of proton shell-structure can be included, quantitatively, in the compressible liquid-drop model of nuclei by the Strutinski procedure (see Ring & Schuck 1980) to obtain formation enthalpies for nuclei in the interval $20 \leq Z \leq 50$. Section 3 gives estimates of the weak-interaction transition rates between these nuclei and, from an initial temperature of 5×10^9 K, which is in the vicinity of the melting temperature or glass transition region of the system, describes how the Z -distribution evolves with temperature and time. It also gives estimates of the very broad range of possible neutrino emissivities associated with these transitions which have so far been neglected in all published calculations of neutron-star cooling.

This paper is concerned with the nature of the crust in isolated neutron stars which lack the long period of mass-accretion of binary systems. Factors such as accretion through fall-back at formation are ignored. Therefore, it does not consider neutron stars in those binary systems where the rate of mass transfer is large enough to replace the whole crust, below and above ρ_{nd} (see Schatz et al 1999). The extent to which the results obtained here may be relevant to such systems is discussed briefly in Section 6. Under the physical conditions considered in the present paper, pycnonuclear reactions were examined previously (Jones 2002) and were found to have negligible transition rates in the solid phase. The reason for this is that the intermediate state formed in a solid by fusion of nuclei with charges Z_1 and Z_2 consists of a monovacancy and a point-defect of charge $Z_1 + Z_2$. At the highest matter density, 8.8×10^{13} g cm $^{-3}$, assumed in Sections 2 & 3, for example, this state has a 17 MeV formation enthalpy. (This assumes that analogues of the standard lattice point-defects exist in amorphous solids, though they may be short-lived at high temperatures.) States with even higher formation enthalpy would result from successive fusion reactions, indicating that processes such as pinning-induced nuclear rod formation (Mochizuki, Oyamatsu & Izuyama 1997) are not significant. However, the direct formation of lower-dimensional nuclear structures at temperatures of the order of 10^{10} K, in a density interval between the spherical nuclear phase and the continuous liquid core of the star, is predicted for many models of nuclear matter (Lorenz, Ravenhall & Pethick 1993; Oyamatsu 1993; but see also Douchin & Haensel 2000). Lorenz et al noted that the geometrical form of these structures would allow weak-interaction transitions but gave no estimate of the neutrino emissivity. For completeness, a brief calculation of this emissivity is given in Section 4. It is less significant than that associated with the region of spherical nuclei.

The density region below ρ_{nd} is reconsidered in Section 5 using the binding energy compilation of Møller, Nix & Kratz (1997), but with inconclusive results for values of Q . It is possible to state only that values $Q \approx 1$ are probable, with $Q \gg 1$ in limited regions. This is not too serious a problem for most neutron star calculations owing to the limited depth of the region below ρ_{nd} . Values of Q computed for $\rho > \rho_{nd}$, the region which occupies most of the crust volume, are given in Table 2 and their significance is considered in Section 6.

2 SHELL EFFECTS IN THE DISTRIBUTION OF FORMATION ENTHALPIES

Formation enthalpies for point-defect structures of impurity nuclei with charge Z_i in an otherwise homogeneous *bcc* lattice of charge Z , were obtained in previous work (Paper I) at densities above ρ_{nd} . The method of calculation followed that used earlier for monovacancies (Jones 1999b), the essence of which was application of the Feynman-Hellmann theorem (Slater 1963) to find the lattice displacements in the vicinity of the defect. Nuclei were described by the compressible liquid-drop model (CLDM) of Lattimer et al (1985) with these authors' Skyrme pseudo-potential for bulk nuclear matter and their expression for the thermodynamic potential per unit area of nuclear surface. Lattice-site displacements in the vicinity of an impurity are determined,

principally, by properties of the high-density relativistic electrons at $\rho > \rho_{nd}$. The Coulomb-electron stress-tensor has isotropic components which are between one and two orders of magnitude larger than the off-diagonal. Also, the inverse of the electron-screening wavenumber is larger than the *bcc* lattice constant. Consequently, lattice-site displacements are such that the electron density, averaged over a volume of the order of the Wigner-Seitz cell, adjusts to values almost exactly equal to the mean electron density of the undisturbed lattice. We refer to Paper I for more complete discussions of these and other features of the formation enthalpy calculations. Our primary assumption about the distribution of formation enthalpies is based on these considerations. It is that the formation enthalpy for a nucleus of charge Z_i in an amorphous heterogeneous solid of mean charge \bar{Z} , or in a liquid with the same nuclear charge distribution, is satisfactorily approximated by that calculated for an impurity nucleus of charge Z_i in a homogeneous lattice of charge \bar{Z} .

The formation enthalpies were given in Paper I with reference to that for the homogeneous lattice charge. With the exclusion of integral multiples of the neutron and electron chemical potentials, they were expressed as $H_{FZ} = C(Z - \bar{Z})^2$ for charge Z . Values of the constant C are given here in Table 1 at several matter densities with, for convenience, the parameters of the lattices concerned. The values of ρ chosen exclude the region immediately above ρ_{nd} because it represents a relatively small interval of depth in the solid crust. The CLDM parameters used by Lattimer et al fit the ground states of laboratory even-even nuclei and so include the effects of pairing interactions. Thus our expression for H_{FZ} neglects shell effects, including the unpaired proton in odd- Z nuclei. The investigation by Negele & Vautherin (1973) revealed a proton shell structure very similar to that of laboratory nuclei. Although shell energy-differences are modified in the neutron continuum, the shell ordering (see Figure 5 of their paper) is changed only in that $1d_{3/2}$ and $1f_{5/2}$ respectively, precede $2s_{1/2}$ and $2p_{3/2}$. We are unaware of any published sequence of single-particle energy levels for nuclei beyond the neutron-drip threshold apart from those contained in that paper. However, Chabanat et al (1998) have shown by calculation of two-neutron separation energies that shell effects at neutron numbers $N = 50, 82$ remain significant immediately below the neutron-drip threshold. There is no doubt that our expression for H_{FZ} ought to be modified by shell structure, but the form of these changes was considered only qualitatively in Paper I.

At matter densities $\rho > \rho_{nd}$, there is a neutron continuum with chemical potential $\mu_n > 0$. It is degenerate, except for a small volume with $\rho \approx \rho_{nd}$, and is superfluid at temperatures $0 < T < T_{cn}^e$. Nuclei can be most simply viewed as bound states of protons embedded in this system, charge-neutralized by an almost uniform relativistic electron gas. The formation enthalpy differences $H_{FZ+1} - H_{FZ}$ can, in principle, be affected by neutron shell-structure because the change in Z will be associated with a change in nuclear radius r_N and, possibly, a change in the number of neutron single-particle states at negative energy. But we shall assume that neutron transitions from the continuum just above the zero of energy to states just below do not contribute to discontinuities in the formation enthalpy differences with which this paper is concerned. Thus we consider the effects of proton shell-structure only, and regard the neutrons within the

nuclear volume as merely a part of the superfluid continuum, though with increased density and a locally modified superfluid energy gap.

Shell effects in the formation enthalpies of nuclei with $20 \leq Z \leq 50$ are estimated here using the Strutinski procedure, following fairly closely the account given by Ring & Schuck (1980). If a purely notional single-particle level sequence were to be associated with the CLDM approximation, its level density would be a monotonic and smoothly varying function of Z or of single-particle energy. Real single-particle level densities are not like this. Thus the procedure starts from a computed level density $g(\epsilon)$ and single-particle energy sum E_{sp} and generates an averaged level density $\tilde{g}(\epsilon)$ and energy sum \tilde{E}_{sp} . Hence the formation enthalpy deviation from its CLDM value at a specific Z is given by

$$H_{FZ} = (H_{FZ})_{CLDM} + E_{sp} - \tilde{E}_{sp} + \epsilon_{pq}. \quad (2)$$

The average of this expression, for even- Z nuclei, over an interval of Z would then be $(H_{FZ})_{CLDM}$, the underlying CLDM formation enthalpy. The correction terms in this expression should, of course, be enthalpies because the weak-interaction transitions occur at constant pressure. But the error in replacing enthalpies by energies here is not large and is certainly less serious than that inherent in the neglect of configuration mixing, to which we shall refer later. The first three terms in the right-hand side of equation (2) give the shell-corrected formation enthalpy for even- Z nuclei. The remaining term, nonzero only for odd- Z nuclei, is the excitation energy of a single proton quasiparticle. The shell-model energy is

$$E_{sp} = \int_{-\infty}^{\lambda} \epsilon g(\epsilon) d\epsilon, \quad (3)$$

where λ is the proton chemical potential and

$$g(\epsilon) = \sum_i \delta(\epsilon - \epsilon_i) \quad (4)$$

is the density of single-particle states. The averaged shell-model energy is given by the Strutinsky-averaged density of states \tilde{g} defined by the averaging procedure

$$\tilde{g}(\epsilon) = \int_{-\infty}^{\infty} g(\epsilon') f\left(\frac{\epsilon - \epsilon'}{\gamma}\right) d\left(\frac{\epsilon - \epsilon'}{\gamma}\right). \quad (5)$$

It is

$$\tilde{E}_{sp} = \int_{-\infty}^{\tilde{\lambda}} \epsilon \tilde{g}(\epsilon) d\epsilon, \quad (6)$$

where the modified chemical potential $\tilde{\lambda}$ remains to be determined. It is clearly necessary that successive applications of the averaging procedure should leave \tilde{g} unchanged. A suitable class of functions satisfying this condition is formed by products of gaussian functions with generalized Laguerre polynomials. We assume a specific order of polynomial,

$$f(x) = \frac{1}{\sqrt{\pi}} e^{-x^2} \left(\frac{15}{8} - \frac{5}{2}x^2 + \frac{1}{2}x^4 \right), \quad (7)$$

and refer to Ring & Schuck for further details and for a tabulation of them. An averaged occupation number \tilde{n}_i is defined for each proton state,

$$\tilde{n}_i = \int_{-\infty}^{\frac{\tilde{\lambda} - \epsilon_i}{\gamma}} f(x) dx \quad (8)$$

Table 1. Properties of CLDM lattice nuclei in equilibrium with a uniform neutron liquid of number density n_n^e . The matter density is ρ , and \bar{Z} is here the uniform nuclear charge, a CLDM continuous variable. The Fermi wavenumbers are p_{Fn} for neutrons within the nuclear volume and p_{Fe} for the electrons. The radii of the nucleus and Wigner-Seitz cell are r_N and r_{WS} , respectively. The lattice Debye and melting temperatures are T_D and T_m . The energy gap of the neutron continuum is Δ_n^e , and C is the formation enthalpy constant.

n_n^e 10^{-3} fm^{-3}	ρ $10^{13} \text{ g cm}^{-3}$	\bar{Z}	p_{Fn} fm^{-1}	p_{Fe} fm^{-1}	r_N fm	r_{WS} fm	T_D 10^9 K	$k_B T_m$ MeV	Δ_n^e MeV	C MeV
7.8	1.6	34.65	1.47	0.231	5.82	27.1	1.8	0.36	0.77	0.0142
18.4	3.7	35.13	1.48	0.286	6.28	22.0	2.3	0.46	1.10	0.0096
43.6	8.8	34.26	1.49	0.363	7.10	17.15	2.9	0.56	0.67	0.0051

and the constraint

$$\sum_i \tilde{n}_i = Z \quad (9)$$

is used to determine the modified chemical potential $\tilde{\lambda}$. The parameter γ defines the width of the averaging function. It is chosen to satisfy, so far as possible, the condition that the averaged energy $\tilde{E}_{sp}(\gamma)$ should be independent of it.

The scheme requires a set of proton single-particle levels ϵ_i . As in Paper I, and in order to make use of the values of the parameter C calculated in that work, we obtain approximate sets of homogeneous *bcc* lattice parameters by using the CLDM approximation, closely following Lattimer et al (1985). These are given in Table 1 and form a basis for our calculation of formation enthalpy differences. For each matter density, we obtain a set of ϵ_i from the work of Negele & Vautherin (1973; fig. 5). Values of the width γ in the interval $2 \leq \gamma \leq 6$ MeV have been investigated. The choice is to some degree a matter of compromise because the stationarity condition is not perfectly satisfied by $\tilde{E}_{sp}(\gamma)$ at a common γ for all Z in the range $20 \leq Z \leq 50$. Thus we have adopted a fixed value $\gamma = 4$ MeV for all sets of ϵ_i . The first three terms in the right-hand side of equation (2) are then calculated from the values of the constant C given in Table 1 and from the procedure described above. The remaining term ϵ_{pq} presents some difficulty. It is recognized that its value depends on the extent to which the shell concerned is filled but for simplicity, we have assumed a constant value for all odd- Z nuclei, with $\epsilon_{pq} = 0$ for even- Z nuclei.

A typical set of H_{FZ} values given by equation (2) is shown in Fig. 1, which is for a matter density $\rho = 3.7 \times 10^{13} \text{ g cm}^{-3}$. The enthalpies exclude integral multiples of the electron and neutron chemical potentials. There are pronounced minima in formation enthalpy at the closed-shell charges $Z = 20, 34, 40, 50$. These minima are also present at the other densities listed in Table 1 though with rather different relative values of formation enthalpy. For the formation of a thermal equilibrium population of nuclei, or for the calculation of weak-interaction transition rates, we require only the differences $H_{FZ+1} - H_{FZ}$. Also shown are $(H_{FZ})_{CLDM}$ values corrected only by the ϵ_{pq} term. Comparison of these two sets confirms that, as suggested in Paper I, shell effects are a more important source of formation enthalpy differences between nuclei of neighbouring Z than the CLDM bulk nuclear matter term.

The fact that the important closed shells are at $Z = 34, 40$ is a consequence of our choice, in Paper I, of the Lattimer et al CLDM which produces $\bar{Z} \approx 35$ in the density interval considered here (see also Pethick & Ravenhall 1995,

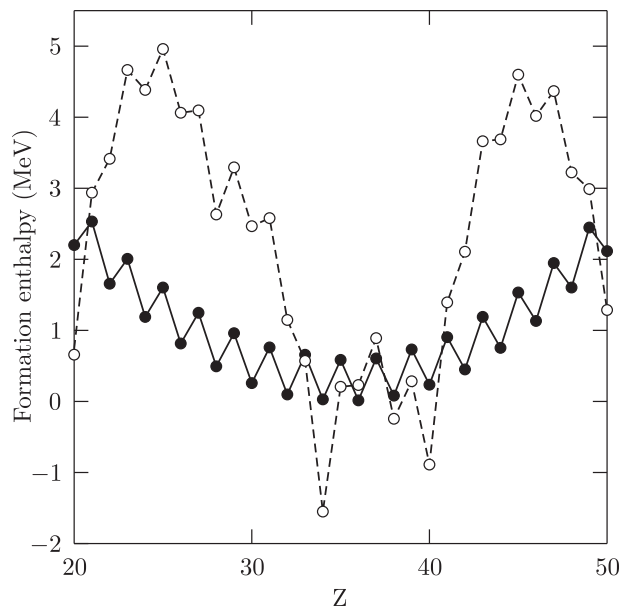


Figure 1. Formation enthalpies H_{FZ} are given for nuclei $20 \leq Z \leq 50$ at matter density $\rho = 3.7 \times 10^{13} \text{ g cm}^{-3}$. Those represented by open circles have been obtained using the Strutinsky procedure whereas the solid circles are the $(H_{FZ})_{CLDM}$ values corrected only for the unpaired proton. In both cases, this term is $\epsilon_{pq} = 0.6$ MeV. In the former case, proton shell closures at $Z = 20, 34, 40, 50$ are associated with very marked enthalpy minima.

Fig. 2). If, instead, the Douchin & Haensel CLDM which gives typically $\bar{Z} \approx 45$ had been used, we anticipate that the general form of Fig.1 would be unchanged except for a displacement to higher Z , with the important closed shells being those at $Z = 40, 50$. The shell effects of this paper have been obtained using a specific scheme of calculation and it is worth considering the extent to which they are physically realistic. The values of ρ concerned are subnuclear so that the definition of single-particle levels, as in free (laboratory) nuclei, is not unreasonable. The form of single-particle wave functions changes completely, owing to spatial quantization, in the progression to a new shell and this is reflected in the level density discontinuity which produces shell effects. But in reality, single-particle or hole states are certainly modified by residual nucleon-nucleon interactions which introduce components of the same angular momentum and parity but with more complex particle-hole structure. Our expectation is that this configuration mixing would change

the relative spacings of the ϵ_i so as to reduce the values of $E_{sp} - \bar{E}_{sp}$ generated by this procedure. Consequently, the extent of shell structure seen in, for example, Fig. 1, should be treated as an upper limit to the true contribution of shell structure to formation enthalpy differences between nuclei of neighbouring Z . A further reason why these results should be regarded as no more than a guide to true formation enthalpy differences is that their Z -average (in Fig. 1) does not appear to conform well with $(H_{FZ})_{CLDM}$, possibly because the CLDM parameters are to some extent inconsistent with the Negele & Vautherin levels.

3 WEAK-INTERACTION TRANSITION RATES AND COOLING

Given the formation enthalpies for nuclei in the interval $20 \leq Z \leq 50$, an estimate of the initial condition as the star cools can be obtained by assuming that, above a certain temperature, weak-interaction transition rates are large enough to maintain approximate local thermal equilibrium. We assume here, quite arbitrarily, that this temperature is $T_0 = 5 \times 10^9$ K. The arbitrary nature of our assumption follows from the difficulty in calculating transition rates at temperatures $T \gtrsim T_0$ where neutrino phase-space occupation numbers cannot be assumed to be zero. It is also necessary to make the simplifying approximation of neglecting nuclear excited states. Individual nuclear partition functions are then equal to $2J + 1$, where the nuclear spin J is derived entirely from the protons. Unpaired neutrons, or neutron quasiparticles at $T < T_{cn}$, are viewed as excitations of the neutron continuum rather than of individual nuclei. The further evolution of the system at $T < T_0$ depends on the specific heat, the neutrino emissivities, and on the set of weak-interaction $Z \rightleftharpoons Z + 1$ transition rates.

Equations (A4)-(A9) of Paper I give the $Z \rightarrow Z + 1$ transition rate from an initial proton closed-shell nucleus. A proton is created in a new shell of angular momentum j with, in the superfluid case at $T < T_{cn}$, either the creation or annihilation of a neutron quasiparticle. The conservation equations for these two energetically distinct processes are

$$\pm \epsilon_n = H_{FZ+1} - H_{FZ} + \epsilon_e + \epsilon_{\bar{\nu}}, \quad (10)$$

in which the electron and neutron energies are measured from their chemical potentials μ_e and μ_n , with $\epsilon_n \geq \Delta_n$, where Δ_n is the neutron energy gap. These are a form of direct Urca transition because the Fourier transform of the proton wave function always has a finite amplitude at the wavenumber $\mathbf{p}_n - \mathbf{p}_e - \mathbf{p}_{\nu}$ necessary for momentum conservation. The transition rate, summed over all states in the new shell, is the product of a rate constant Γ_0 and a phase-space integral (equations A7 and A8). We refer to Paper I for further details. In the more general case of a partially filled shell, the protons are assumed to be paired into states of zero angular momentum. The rate constant Γ_0 is then multiplied by a j -dependent factor. For example, in a $Z \rightarrow Z + 1$ transition in which the shell initially contains two protons, the factor is $(1 - 2/(2j + 1))$. A second $Z \rightarrow Z + 1$ case is that in which the shell initially contains an odd number of protons. For the case of a single proton, the factor is $2/(2j + 1)^2$.

Nuclear spins obtained directly from the Negele & Vautherin shell ordering are assumed in the present paper, but

with some reservation. The sequences of ground-state spins and parities tabulated by Møller et al (1997) for nuclei close to neutron instability, and hence relevant below neutron-drip, are not at all simple, possibly owing to the significant nuclear deformation. It is not obvious that, above neutron-drip, a system of Z protons embedded in a neutron continuum will be without deformation and consequent complexities. But the conclusions which will be described in this Section concerning Z -heterogeneity are so clear that they would not be affected by changes in the detail of shell ordering.

The parameters used in the evaluation of transition rates at a given temperature are those listed in Table 1 except that we assume different neutron energy gaps and critical temperatures in the nuclear interior and in the continuum. The neutron effective mass is $m_n^* = 0.8m_n$. Following a local density approximation (LDA), values of the neutron Fermi wavenumber p_{Fn} and the zero-temperature neutron energy gap Δ_n are those for an infinite system at the density of the nuclear interior. The critical temperature T_{cn} is that for an isotropic BCS superfluid. The finite-temperature energy gap needed for calculation of the phase-space integral is conveniently obtained from tabulated results given by Rickayzen (1965), as is the BCS neutron specific heat. The specific heat of the system has components for the electron gas, the solid, and for the neutrons (normal or BCS superfluid). Although the solid is amorphous and heterogeneous, it is represented by a simple Debye model with a single temperature T_D .

The neutron energy gap in neutron-star matter is not well known. Different methods of calculation lead to a wide range of values, (see the reviews of Pethick & Ravenhall 1995, Heiselberg & Hjorth-Jensen 2000). However, methods that introduce corrections such as medium polarization to the calculation inevitably seem to suppress the energy gap as shown, for example, by Shen et al (2003) who also give a brief review of recent work on this topic. For this reason, we have assumed that the energy gap obtained by Ainsworth, Wambach & Pines (1989) applies to the neutron continuum Δ_n^e . This affects only the specific heat. The neutron energy gap effective in the nuclear interior and the proton quasiparticle energy are even more difficult to estimate in neutron star matter. The neutron coherence length is at least of the same order of magnitude as the nuclear radius, so that the proximity effect is certain to be significant for the neutron gap, as has been emphasized by Pethick & Ravenhall. Hence the value of the LDA assumption must be limited. These authors also observe that pairing in the interior of ordinary nuclei is a kind of proximity effect in that attractive pairing in the relatively large, low-density, surface volume influences pairing in the whole. The absence of this low nucleon-density region owing to the presence of the neutron continuum may then affect the proton pairing ϵ_{pq} . The uncertainties of prediction are such we think it necessary to treat the interior neutron energy gap and the proton quasiparticle energy as unknown parameters which are both assumed to be within the interval $0 < \epsilon_{pq}, \Delta_n < 1$ MeV.

Routines for the evaluation, at any temperature, of the specific heat and of all transition rates for $20 \leq Z \leq 50$ with the proton level sequence $1f_{7/2}, 1f_{5/2}, 2p_{3/2}, 2p_{1/2}, 1g_{9/2}$ allow the change in Z -distribution to be followed as the star cools. They also give the neutrino emissivity. We have

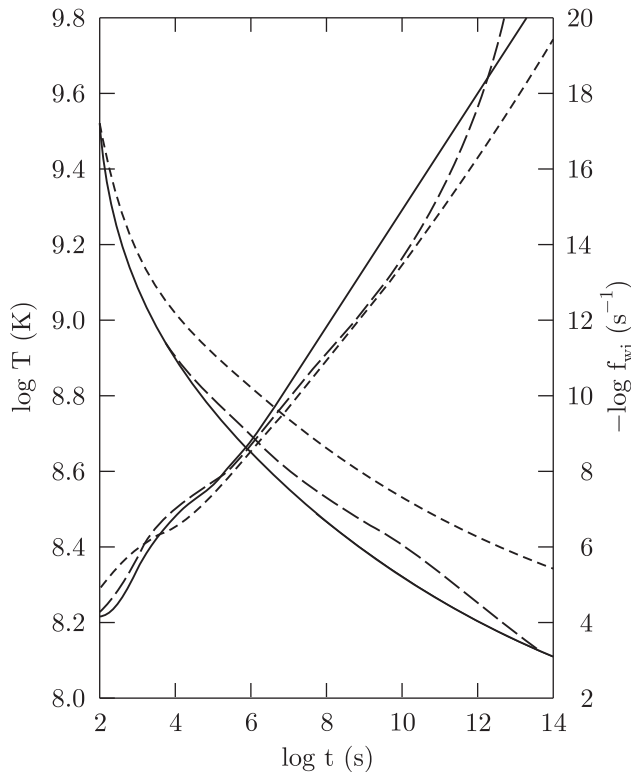


Figure 2. The left-hand set of curves shows the cooling as a function of time at a matter density of $3.7 \times 10^{13} \text{ g cm}^{-3}$ for formation enthalpies given by the solid circles of Fig. 1. The cooling is adiabatic except for the neutrino and antineutrino emissivities described by equation (10). Neutrino pair production by electron bremsstrahlung and by neutron quasiparticle annihilation are neglected here. Allowance for these processes would produce faster cooling, particularly at $t \gtrsim 10^{10} \text{ s}$. The right-hand curves measure the movement of nuclear charge (the flux f_{wi} per unit nucleus) from $Z = 40$ toward the closed shell at $Z = 34$ as a consequence of the weak interaction. It is a function of temperature, but is represented in the figure as a function of time by means of the left-hand set of curves. The product tf_{wi} is always some orders of magnitude smaller than unity, showing that the movement of charge during cooling is insignificant. The solid, large and small-dashed curves are, respectively, for the parameter sets: $\Delta_n = 0.2$, $\epsilon_{pq} = 0.4 \text{ MeV}$; $\Delta_n = 0.4$, $\epsilon_{pq} = 0.4 \text{ MeV}$; $\Delta_n = 0.4$, $\epsilon_{pq} = 0.6 \text{ MeV}$.

adopted an arbitrary fixed initial temperature $T_0 = 5 \times 10^9 \text{ K}$, which is close to the *bcc* lattice melting temperatures given in Table 1. The cooling curves for a matter density of $3.7 \times 10^{13} \text{ g cm}^{-3}$ (adiabatic except for neutrino and antineutrino emission through the processes described by equation 10) are shown in Fig. 2. for the set of H_{FZ} values given in Fig.1 which have no shell correction except for the ϵ_{pq} unpaired-proton term. Three sets of the parameters ϵ_{pq} and Δ_n are considered. The early parts of these curves are not entirely reliable because our calculations neglect neutrino opacity and so overestimate transition rates and emissivities at temperatures significantly above 10^9 K . The right-hand scale gives a measure of how rapidly, at any given temperature, the weak interaction is changing the nuclear Z -distribution by moving nuclei between two of the minima in Z which appear in Fig. 1. It shows the flux f_{wi} between $Z = 40$ and $Z = 34$, calculated at $Z = 37$ and

Table 2. Values of the impurity parameter Q and mean charge \bar{Z} : $Q = Q_{sc}$ with shell corrections; $Q = Q_{nsc}$ with no shell corrections.

ρ $10^{13} \text{ g cm}^{-3}$	Q_{sc}	\bar{Z}_{sc}	Q_{nsc}	\bar{Z}_{nsc}
1.6	12	37.8	5	34.6
3.7	6	35.3	17	33.8
8.8	19	39.0	24	34.4

normalized per unit nucleus in the system, for the cooling conditions assumed here. This quantity is a function of temperature, apart from a relatively small dependence on the changing Z -distribution. It is given here as a function of time by using the left-hand sets of curves in the Figure. Using the (right-hand) sets of curves so obtained, it can be seen that the product tf_{wi} is always some orders of magnitude smaller than unity. (Fig. 2 allows recovery of f_{wi} as a function of T so that it is possible to estimate the time required for weak-interaction equilibrium at a fixed temperature.) Weak-interaction rates are so low that even with the extreme assumption of no shell corrections, the distributions of fractional concentrations for even- Z nuclei change very little with time provided $\epsilon_{pq} \geq 0.4 \text{ MeV}$. In the limit of large t , the resulting values of the impurity parameter Q are not much smaller than those ($Q = Q_m$ in Table 2 of Paper I) for thermal equilibrium at the melting temperatures without shell corrections and with $\epsilon_{pq} = 0$. They are shown here in Table 2. In the shell correction cases, there is naturally some movement of Z toward the magic numbers but the resulting values of Q are independent of Δ_n and ϵ_{pq} to such an extent that, given the very approximate nature of our calculations, it is not useful to include in the tabulation the values of these two parameters used, which are those of Figs. 4-6. The same comment can be made for the no shell-correction cases provided, as we stated previously, that $\epsilon_{pq} \geq 0.4 \text{ MeV}$. Lower values of this parameter, in the special case of the absence of shell corrections, produce potential barriers small enough to allow movement of Z toward \bar{Z} . But we do not attempt to give Q -values for this set of assumptions which are very unlikely to be physically realized. The Q -values of Table 2 and their significance will be considered further in Section 6. But it is not realistic to neglect shell effects completely. These must be present although, owing to uncertainties such as configurational mixing (Section 2), the formation enthalpy differences they introduce may be smaller than those shown in Fig.1. Thus the potential barriers in the weak-interaction paths between the closed shells at $Z = 20, 28, 34, 40, 50$ must be much higher than assumed in our calculations of f_{wi} , and the actual values of f_{wi} many orders of magnitude smaller as a consequence.

Sets of curves similar to those of Fig. 2 exist for the other densities listed in Table 1. But they are so similar that they are not shown here. Our conclusion is that, even with allowance for the uncertainties inherent in the shell-effect formation enthalpy differences calculated here, solid neutron-star matter cools to a system heterogeneous in Z . Other sources of error are much less significant. For example, the Bessel function bound-proton states assumed in equations (A4)-(A6) of Paper I must overestimate the true transition rates, as would our neglect of neutrino opac-

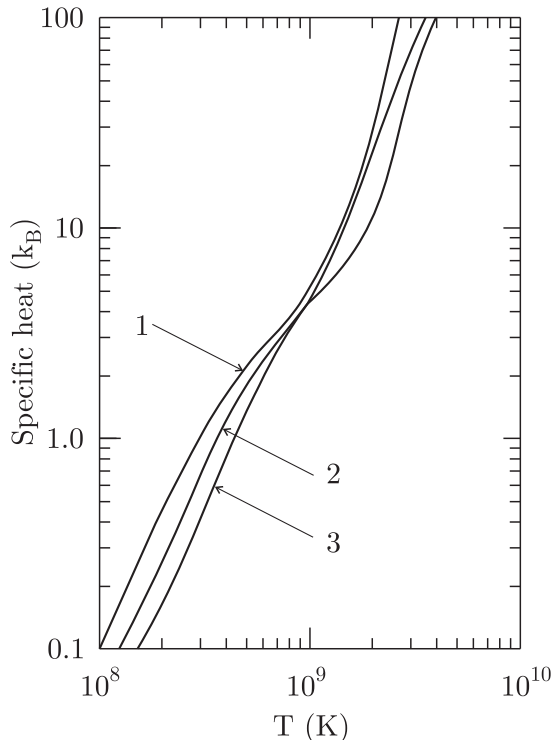


Figure 3. The specific heat per average Wigner-Seitz cell is shown as a function of temperature, in units of k_B . The curves labelled 1 – 3 are, respectively, for matter densities $1.6, 3.7,$ and $8.8 \times 10^{13} \text{ g cm}^{-3}$. The neutron continuum energy gaps Δ_n^e are those given in Table 1. The internal gap $\Delta_n = 0.2 \text{ MeV}$.

ity at $T > 10^9 \text{ K}$. But modest errors are not important because these transition rates determine both the cooling and change in Z -distribution of the system. Very broadly, we can see that a sufficient condition for maintaining Z -heterogeneity during cooling is that the thermal energy per average Wigner-Seitz cell should be smaller than the mean energy, of the order of $6k_B T$, removed by neutrinos or antineutrinos in a weak transition. The specific heat per average Wigner-Seitz cell is shown in Fig. 3 as a function of temperature. It demonstrates that the thermal energy satisfies this condition easily at $T \lesssim 10^9 \text{ K}$ but not at $T \gg 10^9 \text{ K}$ (the neutron contribution is large at $T \gtrsim T_{cn}^e$). It is also true that we have neglected other well-established sources of neutrino emissivity which, if included, would cool the system more quickly and so assist in maintaining heterogeneity.

The neutrino emissivities are shown in Figs. 4-6 for the matter densities listed in Table 1. In each case, they are given both with and without the Strutinsky shell corrections obtained here and for sets of values of ϵ_{pq} and Δ_n . The principal well-established neutrino-emissivity processes, for the inner crust, in studies of neutron-star cooling are neutrino-pair production by electron bremsstrahlung and by neutron quasiparticle annihilation in the superfluid. We emphasize that these emissivities have not been included in our cooling calculations but, for reference purposes, they are shown separately, obtained from Fig. 4 of the paper by Kaminker, Yakovlev & Gnedin (2002). Obviously, the potential barriers which separate formation enthalpy minima at closed shells are of crucial importance in determining emissivities. It is

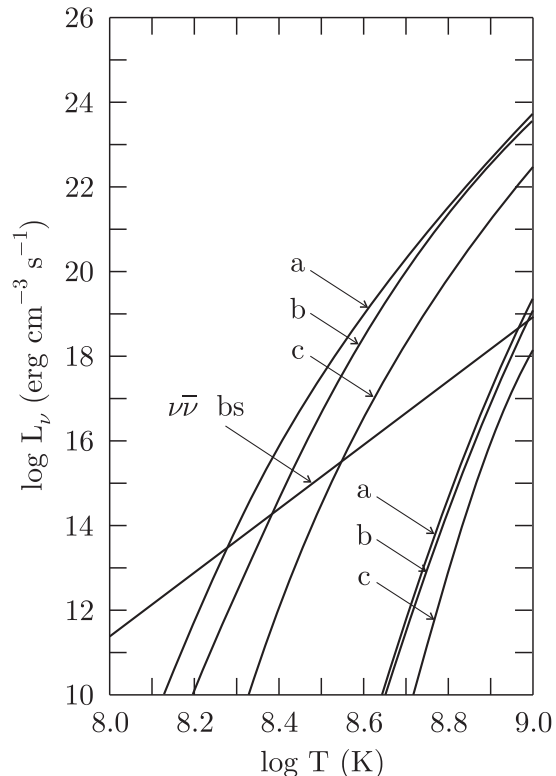


Figure 4. Neutrino emissivities at a matter density of $1.6 \times 10^{13} \text{ g cm}^{-3}$ are shown as functions of temperature for the weak-interaction processes described by equation (10). The formation enthalpies are obtained by the inclusion of shell corrections (lower set of curves) and without these corrections (upper set of curves). Neutrino-pair production by electron bremsstrahlung and neutron quasiparticle annihilation are excluded from these curves, but their emissivity is shown separately for reference purposes. The curves labelled $a - c$ are, respectively, for the following parameter sets: $\Delta_n = 0.2, \epsilon_{pq} = 0.4 \text{ MeV}$; $\Delta_n = 0.4, \epsilon_{pq} = 0.4 \text{ MeV}$; $\Delta_n = 0.4, \epsilon_{pq} = 0.6 \text{ MeV}$.

possible to say with confidence only that the emissivities shown are likely to form upper and lower bounds for the true values. As they differ by at least several orders of magnitude, this is not a very strong or practically useful statement. But given that the solid inner crust is heterogeneous in Z , the existence of this source of uncertainty must be accepted. Its effect on the surface temperature of the star is difficult to estimate without complete cooling calculations.

4 LOW-DIMENSIONAL STRUCTURES

Phases in which protons are confined to one or two-dimensional structures have been studied extensively and their existence in a substantial density interval between the spherical nuclear phase and the liquid core depends on the form of the Skyrme pseudopotential assumed in deriving the equation of state. Both Lorenz et al (1993), using the interaction of Lattimer et al, and Oyamatsu (1993) find such structures within a significant density interval. A survey of work on this topic has been given by Pethick & Ravenhall (1995). But more recent calculations by Douchin & Haensel (2000), using a different Skyrme interaction, find only the

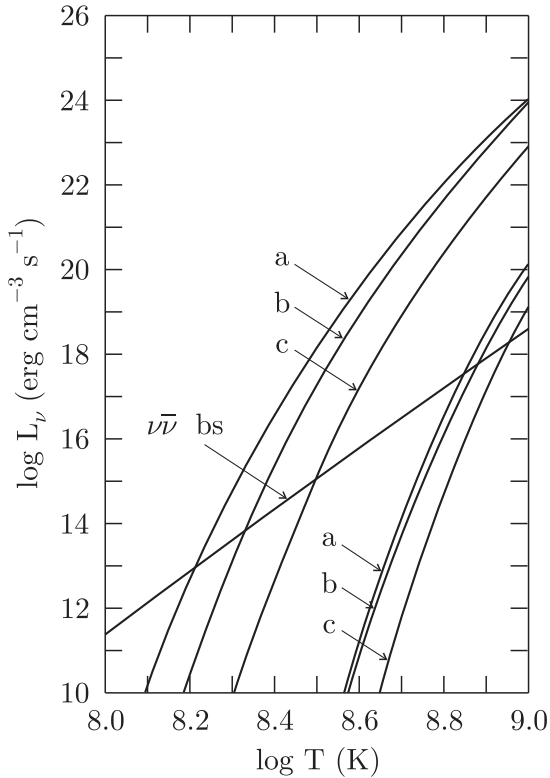


Figure 5. Neutrino emissivities at a matter density of $3.7 \times 10^{13} \text{ g cm}^{-3}$ are shown with labelling and parameter sets as for Fig. 4.

phase of spherical nuclei. Investigations since then (Watanabe & Iida 2003) have shown that the inclusion of electron screening tends to increase the density interval occupied by any such phase. The paper by Lorenz et al notes that these structures give rise to new weak-interaction processes but gives no further details. These are no more than a different form of the direct Urca transition considered in Section 3. For completeness, the neutrino emissivity has been calculated here for one of these cases, allowing a comparison with the range of emissivities obtained for the spherical nuclear phase. The one-dimensional system considered is that in which the Wigner-Seitz cell is an infinite slab of thickness $2d_{WS}$ containing neutrons and relativistic electrons. Protons are confined within a slab of thickness $2d_N$ symmetrically positioned inside this cell. Thus the component of the proton wave function in the variable perpendicular to the slab has Fourier transform ψ_m with quantum number m and finite amplitude at the wavenumber necessary for momentum conservation. We assume that, with this limitation, neutrons and protons each form an isotropic BCS superfluid, with energy gaps $\Delta_{n,p}$. The neutrino emissivity per unit volume is then

$$L_{s\nu} = \frac{(1 + 3C_A^2)G^2 \cos^2 \theta_c}{(2\pi)^{11} \hbar d_{WS}} \int d^3 p_n d^2 q d^3 p_e d^3 p_\nu \sum_m |\psi_m(p_{n\perp} - p_{e\perp})|^2 \delta^{(2)}(\mathbf{p}_n - \mathbf{p}_e - \mathbf{q}) \sum \epsilon_\nu u_n^2 v_p^2 n_n (1 - n_p)(1 - n_e) \delta(\epsilon_n - \epsilon_p - \epsilon_e - \epsilon_\nu). \quad (11)$$

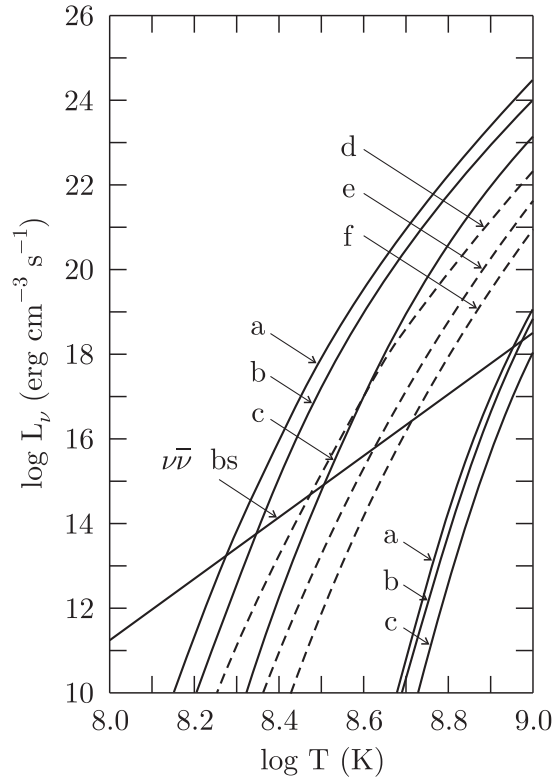


Figure 6. Neutrino emissivities at a matter density of $8.8 \times 10^{13} \text{ g cm}^{-3}$ are shown with labelling and parameter sets as for Fig. 4. The additional set of broken curves are the neutrino emissivity $L_{s\nu}$ given by equation (11) for a one-dimensional slab nuclear structure. The curves labelled $d - f$ are, respectively, for the parameter sets: $\Delta_n = 0.2, \Delta_p = 0.4 \text{ MeV}$; $\Delta_n = 0.4, \Delta_p = 0.4 \text{ MeV}$; $\Delta_n = 0.4, \Delta_p = 0.6 \text{ MeV}$.

In this expression, G is the muon decay constant, θ_c is the Cabibbo angle, and $C_A = 1.25$ is the ratio of axial vector to vector coupling constants. The wavevector \mathbf{q} lies in the plane of the slab. The neutrino or antineutrino energy is ϵ_ν . Quasiparticle or electron occupation numbers are $n_{n,p,e}$ and $\epsilon_{n,p,e}$ are the energies, referred to the chemical potential. The Bogoliubov coefficients for the proton and neutron quasiparticle states are u_n and v_p . The terms shown in this expression are for the process of neutron quasiparticle annihilation with proton quasiparticle and electron creation. However, the unlabelled summation states that the set of 8 terms, derivable from the creation or annihilation of the electron and of the neutron and proton quasiparticles, are included.

Numerical evaluation of this somewhat untidy expression gives the emissivities shown in Fig. 6 for a matter density of $1.59 \times 10^{14} \text{ g cm}^{-3}$ ($d_N = 3.62 \text{ fm}$, $d_{WS} = 10.1 \text{ fm}$) for several sets of values of $\Delta_{n,p}$. Values of the emissivity do not vary greatly with matter density in this phase or with the parameter d_N which is itself very much dependent on CLDM details. Emissivity calculations with different values of d_N show that uncertainties arising here are small compared with those caused by our lack of knowledge of the energy gaps $\Delta_{n,p}$. In general, the emissivities are rather smaller than those found in the spherical nuclear phase, the reason

being that the Fourier transforms of the proton states in that phase have broader distributions of momentum.

5 THE OUTER CRUST

The canonical crust structure at densities $\rho < \rho_{nd}$ is obtained by minimization of the Gibbs free energy per nucleon. It consists of successive spherical shells, each of a *bcc* lattice homogeneous in the nuclear charge Z neutralized by a relativistic electron gas. The most recent calculations are those of Haensel & Pichon (1994) who also review earlier work. The zero-temperature structure of the interfaces between these shells was examined by Jog & Smith (1982) and found to consist of extremely thin layers of interpenetrating simple cubic lattices of the two nuclear charges concerned. Formation, however, must be considered at the lattice melting temperature T_m , or above. The reduction in free energy, derived from the melting temperature entropy of mixing for the two nuclear species, then gives interface layers of significant thickness in which one nuclear species is present as an impurity in a lattice formed by the other (De Blasio 2000).

Consideration of the later stage of nuclear formation at finite temperature gives quite separate grounds for excluding homogeneous lattices (Jones 1988). At temperatures in the vicinity of T_m , nuclei are in state of partial thermal equilibrium with the electrons and with a low-density Boltzmann gas of neutrons. (Weak-interaction transition rates, even at T_m , are too small to guarantee equilibrium Z -values, but the transition rates for the emission or absorption of neutrons are high and so maintain strong-interaction equilibrium with the Boltzmann gas at any density.) From the definition of the neutron-drip density ρ_{nd} , the neutron chemical potential in this region is $\mu_n = \mu_n^e < 0$, referred to the rest energy as zero. The equilibrium number density of the Boltzmann gas is

$$n_n^e = \frac{2}{\lambda_n^3} \exp(\beta \mu_n^e), \quad (12)$$

where

$$\lambda_n = \sqrt{\frac{2\pi\beta\hbar^2}{m_n}}, \quad (13)$$

and $\beta^{-1} = k_B T$. Thus it decreases rapidly as the star cools. But the nature of the system imposes an additional constraint on the Gibbs function minimization. The neutron scattering cross-section is so large that, once nuclei have formed, diffusion over macroscopic distances of the order of the shell depth is not possible within the short time permitted by neutron condensation on to nuclei. This occurs at a temperature $\tilde{T} > T_0$, where T_0 is the temperature (not well-defined) at which weak-interaction equilibrium fails. Consequently, it is necessary to impose the further condition, at temperatures $T \lesssim T_m$, that the mean nucleon number A_{WS} , per Wigner-Seitz cell, should be constant. We refer to Jones (1988) for further details.

The method of calculating equilibrium nuclear number densities differs from that of Paper I which was for densities above ρ_{nd} . The pressure at $\rho < \rho_{nd}$ is small in nuclear structure terms, being almost entirely that of the degenerate electron gas. Nuclei in this region have definite A, Z and can be assumed to have binding energies $B(A, Z)$ identical

with those of the free (terrestrial) state. The minimization of the Gibbs function G for a fixed number of baryons is at constant μ_e and hence approximately at constant pressure. It is,

$$\frac{\partial}{\partial n_{ij}} \left(G + \Lambda \sum_{ij} n_{ij} \right) = 0, \quad (14)$$

where n_{ij} is the number of nuclei with mass number A_i and charge Z_j , and Λ is a Lagrange multiplier. The equilibrium condition for the nuclear chemical potential $\tilde{\mu}_{ij}$ is,

$$\tilde{\mu}_{ij} + (A_{WS} - A_i)(\mu_n^e + k_B T) + Z_j \mu_e + \Lambda = 0. \quad (15)$$

(Without the constant A_{WS} constraint, the nuclear chemical potential would be $\tilde{\mu}_{ij} = A_i \mu_n^e - Z_j \mu_e$.) The neutron chemical potential is not an independent variable in equation (15): it is a function of A_{WS} through the relation $A_{WS} - \bar{A} = n_n^e V_{WS}$, in which \bar{A} is the mean nuclear mass number and V_{WS} the Wigner-Seitz cell volume. To a satisfactory approximation, the nuclei are independent systems and their equilibrium number densities are given by an expression entirely analogous with equation (12),

$$n_{A,Z} = \frac{\mathcal{Z}}{\lambda_{A,Z}^3} \exp(\beta(\tilde{\mu}_{ij} + Z(m_n - m_p) + B - E_{WS})), \quad (16)$$

where \mathcal{Z} is the nuclear partition function (normalized so that at $T = 0$ it is $2J + 1$), B is the nuclear ground-state binding energy, and E_{WS} is the Coulomb energy of the Wigner-Seitz unit cell. The presence of Λ allows two finite number densities in the zero-temperature limit, as is necessary because A_{WS} is in general not an integer. Evaluation of equation (16) at a standard temperature T_0 , close to T_m , for even-even nuclei with $\mathcal{Z} = 1$ and binding energies from the recent compilation of Møller et al (1997) gives estimates of the mass number and charge heterogeneity expected at densities below ρ_{nd} .

It is unfortunate that the results are inconclusive. The source of the problem is that the values of A_{WS} are determined at those temperatures $\tilde{T} > T_0$ existing at the formation of nuclei, which are high and poorly known. The bulk transport of neutrons over macroscopic distances, of the order of shell depths, is not possible in the short time which elapses before rapid cooling produces almost complete condensation through nuclear capture (Jones 1988). It has to be accepted that the values of A_{WS} , constant at $T < \tilde{T}$, are virtually unknown. Evaluations of equation (16) for matter densities $\rho \sim 1 - 3 \times 10^{11} \text{ g cm}^{-3}$, temperatures $T_0 = 5 \times 10^9$ and 10^{10} K , and a wide range of values of $A_{WS} - \bar{A}$ give a common picture. As $A_{WS} - \bar{A}$ increases, the equilibrium nuclei change from a group associated with the neutron $N = 50$ closed shell to a group near $N = 82$. The neutron chemical potentials at changeover vary from -1.3 MeV at $3 \times 10^{11} \text{ g cm}^{-3}$ to -3.6 MeV at $1 \times 10^{11} \text{ g cm}^{-3}$, for $T_0 = 5 \times 10^9 \text{ K}$. The corresponding values at 10^{10} K are -1.8 and -4.1 MeV , respectively. The changeover from $N = 50$ to $N = 82$ is similar to that found by Haensel & Pichon (1994) in their study of zero-temperature equilibrium. The problem is that the A_{WS} constraint which was not considered by them does not permit us to estimate where it occurs. This complexity is unfortunate, but we believe that it is real. Qualitatively, the consequences for Q -values are as follows. The $N = 50$ region has $Q \ll 1$, and the $N = 82$ region, $Q \sim 1$. Values

$Q \gg 1$ exist in the changeover region owing to the very large differences in Z which are present there, as found earlier by De Blasio (2000). Detailed calculations of weak-interaction transition rates confirming the absence, at $T < T_0$, of weak-interaction equilibrium have not been made for $\rho < \rho_{nd}$, but the qualitative criterion given in Section 3 is satisfied. In particular, values $Q \gg 1$, where they exist, will certainly remain frozen in.

6 TRANSPORT COEFFICIENTS AND CONCLUSIONS

The main conclusion of this paper is that nuclear-charge heterogeneity exists in the solid phase of isolated neutron stars. There must be many reservations about the procedures described in Sections 2 & 3 which have been used to obtain this result. We attempt to summarize them here and in each case give reasons why they should not be viewed as serious. Firstly, the shell-corrected formation enthalpy values, H_{FZ} , are based on the Negele & Vautherin shell ordering and spacings. Nuclei close to neutron-instability are known to be deformed, with ground states of some complexity (see Møller et al 1997). It is quite possible that these features are also present above ρ_{nd} . Therefore, the values shown in Fig. 1 may not give a true picture of the potential barriers which slow weak-interaction transitions. But it is the case that even quite small barriers slow weak transitions sufficiently. The transition rate calculations, following the procedure of Paper I, are based on elementary single-particle proton wave functions and neglect Coulomb corrections to the electron function, which are only moderate at the values of μ_e considered. But here, the effect of more complex ground states would inevitably be reductions in transition rates which would be largely neutral in effect because the rate of cooling by neutrino emission is also reduced. The results, of which those in Fig. 2 are an example, show that the failure of weak-interaction equilibrium during cooling at $T < T_0$ is so clear that the above uncertainties are not significant. The choice of $T_0 = 5 \times 10^9$ K as the lowest temperature at which complete equilibrium remains is, of course, arbitrary. There is no doubt that a higher value would give more heterogeneity in Z , with larger values of Q , and that calculations made by the present methods would show a failure of weak-interaction equilibrium at temperatures below it. But at these very high temperatures, the neutrino opacity would cease to be negligible, as assumed in Section 3, so that the cooling rates shown in Fig. 2 would be overestimates. Obviously, the Q -values given in Table 2, under different stated assumptions, for each of the matter densities listed in Table 1, should be seen as little better than order of magnitude estimates. But these satisfy $Q \gg 1$ in a way which does not depend systematically on the details of shell effects assumed. They are some orders of magnitude larger than the values $Q \ll 1$ previously assumed in the standard view of solid neutron-star matter. Although the relevant calculations have not been made, we suggest there is no reason to think that this conclusion would be changed by replacing the Lattimer et al CLDM with that of Douchin & Haensel (2001). In the latter case, the important proton closed shells would be those at $Z = 40, 50$ but we anticipate that the

orders of magnitude of the Q -parameter obtained would be the same.

The procedures of Sections 2 & 3 are concerned merely with establishing Z -heterogeneity. The small-scale structure of the solid is a different question. It is not obvious that diffusion at temperatures in the glass transition region, which we assume to be near the homogeneous lattice melting temperature T_m , could produce localized order extending over linear dimensions much greater than 10^{1-2} inter-nuclear separations. The results of rudimentary formation enthalpy calculations given in Paper I do not indicate that large chemical potential gradients exist to drive such diffusion. Moreover, the classical entropy of disorder remains large. For these reasons, it is believed that although the structure may not be exactly that of an amorphous heterogeneous solid, any local order will be at most of small linear dimension, analogous with nanostructures in ordinary amorphous matter.

These conclusions can be compared with those of recent work on neutron stars in binary systems with high mass transfer rates, $\gtrsim 10^{-8} M_\odot \text{ yr}^{-1}$ (Schatz et al 1999, see also Brown & Bildsten 1998). Stable burning of hydrogen and helium occurs near the surface, the most important process being rapid proton capture, and is almost complete at a depth of the order of 10^8 g cm^{-3} (see Schatz et al, Fig.1). The end products have charge distributions which depend on the mass-transfer rate, but are typically broad, with $Z \leq 40$. Continued mass-accretion forces these nuclei to higher matter densities, eventually to $\rho > \rho_{nd}$. Schatz et al contrast this Z -heterogeneous matter with the solid phase of an isolated (primordial) neutron star having the properties described by Pethick & Ravenhall (1995). Our conclusion is that the solid phases of neutron stars in these different environments are broadly similar, with impurity parameters $Q \gtrsim 10$. It is very unlikely that the temperatures of the burning processes will be high enough to produce weak-interaction equilibrium at matter densities above ρ_{nd} . The flux f_{wi} , representing the movement of nuclear charge toward a closed proton shell, is shown in Fig. 2 for the case of no shell correction, apart from the proton pairing term ϵ_{pq} . This extreme case is not realistic because there is almost certainly some shell correction, though perhaps not so large as that shown in Fig. 1. The increased potential barriers introduced by the correction would reduce values of f_{wi} by many orders of magnitude, to an extent that Z -heterogeneity would be largely unaffected.

It is obvious that the amorphous and heterogeneous nature of the solid phase of neutron-star matter has significant consequences for its mechanical properties and, above ρ_{nd} , for its interaction with superfluid neutron vortices. Mechanical properties will not be considered here except to note that the response to stress is not strictly that of an ordinary amorphous solid because neutron-star matter is very far from being absolutely stable and therefore cannot exhibit brittle fracture (Jones 2003). Superfluid neutron vortices interact with nuclei through elementary pinning forces whose calculation is associated with unresolved problems (for a brief partial review, see Jones 2002). It is currently not possible to say that the signs or orders of magnitude are known with any degree of certainty at a given matter density. Both vortex pinning and the dissipative force acting on a moving vortex are strongly influenced by the

structure of the solid phase. Apart from the kind of low-dimensional structure considered in Section 4, very small dissipative forces would be possible only for motion through a system of large single crystals with very low concentrations of dislocations and point-defects. The confirmation of the amorphous and heterogeneous nature of the solid phase rules out this possibility.

The neutrino emissivity from nuclear weak interactions at matter densities below ρ_{nd} has not been calculated owing to the difficulty in knowing the correct transition rates between nuclei which are close to being neutron-unstable. The assumption of superallowed Fermi transitions gives an order of magnitude of 10^{22} erg cm⁻³ s⁻¹ at 10^9 K for matter densities $1 - 3 \times 10^{11}$ g cm⁻³, but allowance for the forbidden nature of the transitions would probably reduce this to an emissivity not much different from that for neutrino-pair production by electron bremsstrahlung under these conditions (10^{18} erg cm⁻³ s⁻¹; see, for example, Gnedin et al 2001). Neutrino emissivity above ρ_{nd} is shown in Figs. 4-6. Weak-interaction transitions in this region involve the creation or annihilation of quasiparticles in the neutron continuum. Rate calculations are more straightforward in this case, but owing to the uncertainties in formation enthalpy differences considered above and in Section 2, the emissivities shown in the two sets of curves probably form upper and lower bounds for the true values. However, at temperatures $T \gtrsim 4 \times 10^8$ K, they can be larger than those previously assumed. The degree of uncertainty here is unfortunate but it does seem right that its existence should be recognized in neutron star cooling calculations. Neutrino emissivities for one-dimensional layer structures (Section 4) are also subject to some uncertainty, but are rather smaller than for the spherical nucleus phase considered in Section 3. Emissivities for a two-dimensional phase have not been calculated, but are probably of a similar order of magnitude to those for one dimension.

Electron scattering in a Z -heterogeneous system contributes electrical and thermal resistivities which are related by the Wiedemann-Franz law and are proportional to Q . The corresponding electrical conductivity (for zero magnetic flux density) is, for relativistic electrons at $\rho \gtrsim 10^7$ g cm⁻³,

$$\sigma_i = \frac{\bar{Z}c\mu_e}{4\pi e^2 Q \Lambda_{imp}}, \quad (17)$$

in which the parameter $\Lambda_{imp} \approx 2.03$ in the ultra-relativistic case (see Urpin & Yakovlev 1980, Itoh & Kohyama 1993) and \bar{Z} is the mean nuclear charge. For the values of Q obtained here, the relaxation time underlying equation (17) is so short that its product with the electron cyclotron angular frequency exceeds unity only for magnetic fields $B \gtrsim 10^{13}$ G. Therefore, there is no need to distinguish between longitudinal and transverse components of the conductivity tensor, except at $B \gg 10^{13}$ G. The conductivity is also classical rather than quantum in nature at densities of the order of ρ_{nd} or above (see Potekhin 1999). The electron thermal conductivity κ_i is given, in terms of σ_i , by the Wiedemann-Franz law. These transport coefficients are of importance, in most cases, at very different times during neutron-star cooling. The thermal conductivity κ is usually of interest at early times before the interior of the star, defined for this purpose as matter densities $\rho \gtrsim 10^7$ g cm⁻³, becomes approximately

isothermal. The Q -dependent resistivity obtained here decreases κ , but the significance of the change is not immediately obvious and would require complete neutron-star cooling calculations for its investigation. At later times, internal temperature gradients are very small and it is possible that the consequent changes in them would be relatively unimportant.

The electrical conductivity σ is obtained by combining σ_i with the phonon-scattering conductivity σ_{ph} . The assumption of a homogeneous *bcc* lattice with a low point-defect density gives $\sigma \approx \sigma_{ph}$. Useful summaries of the properties of σ_{ph} for such a system has been given by Urpin & Muslimov (1992) and by Pethick & Sarling (1995). Umklapp processes are by far the more important contribution to resistivity but become energetically disallowed at temperatures $T \lesssim T_U$, where

$$T_U = 2.2 \times 10^8 \rho_{14}^{1/2} \left(\frac{Z}{60}\right)^{1/3} \left(\frac{10Z}{A}\right) \text{ K} \quad (18)$$

and ρ_{14} is the matter density in units of 10^{14} g cm⁻³. At temperatures $T_U < T \ll T_D$, where T_D is the Debye temperature,

$$\sigma_{ph} = 5.5 \times 10^{23} \rho_{14}^{7/6} \left(\frac{10Z}{A}\right)^{5/3} T_9^{-2} \text{ s}^{-1}, \quad (19)$$

whereas in the limit $T \ll T_U$,

$$\sigma_{ph} = 2.1 \times 10^{28} \rho_{14}^{8/3} \left(\frac{10Z}{A}\right)^{14/3} T_9^{-5} \text{ s}^{-1}. \quad (20)$$

In the neutron-drip region $\rho > \rho_{nd}$, the best value of the mass number A , on which the phonon spectrum depends, is not at all obvious. Pethick & Sarling suggest $A = A_{WS}$ but give no reasons why this choice should be suitable for superfluid neutrons at $T < T_{cn}^e$. This factor introduces considerable uncertainty in the form of the function $\sigma_{ph}(T)$. It is also true that the modified phonon spectrum of an amorphous solid must produce substantial changes from equations (18) to (20). These have not been investigated here because, for the amorphous and Z -heterogeneous solid, the impurity resistivity is large so that $\sigma_i < \sigma_{ph}$ except at temperatures $T \gtrsim 10^9$ K. For comparison with equations (19) and (20), evaluation of equation (17) gives a conductivity

$$\sigma_i = 2.0 \times 10^{24} \left(\frac{\bar{Z}\rho_{14}}{A_{WS}}\right)^{1/3} \left(\frac{\bar{Z}}{Q}\right) \text{ s}^{-1}. \quad (21)$$

The values of Q given in Table 2 lead to high impurity resistivity which is only weakly-dependent on A_{WS} . The fact that it is also temperature-independent removes a substantial degree of uncertainty from any model calculations made with it.

Thus the (zero-field) electrical conductivity in most of the inner-crust volume is $\sigma \approx 10^{24}$ s⁻¹ at all times. This is particularly relevant to studies of the evolution of neutron-star magnetic fields which include both the Hall effect, with the possibility of a cascade to high wavenumber field components, and ohmic dissipation (see Hollerbach & Rüdiger 2002 and Geppert & Rheinhardt 2002, who also review earlier work on this problem). The Hall parameter considered by Hollerbach & Rüdiger is

$$\frac{\sigma B}{n_e e c} = 2.3 \times 10^{-3} B_{12} \left(\frac{A_{WS}}{\bar{Z}\rho_{14}}\right)^{2/3} \left(\frac{\bar{Z}}{Q}\right), \quad (22)$$

where n_e is the electron density and B_{12} the magnetic flux density in units of 10^{12} G. It exceeds unity only for $B \gtrsim 10^{14}$ G. The impurity resistivity found here is also relevant for any process in which the field distribution in the solid crust develops high-multipole components by mass-accretion or by flux expulsion from a superconducting neutron-star interior, or for models in which it is confined to the crust (see Page, Geppert & Zannias 2000, who also give an account of previous work on distributions of this kind). Field components of wavelength $2h$ decay ohmically with an exponential time-constant

$$t_c = \frac{4\sigma h^2}{\pi c^2} \quad (23)$$

which, for $h = 10^5$ cm, is only 4.5×10^5 yr, a time small compared with those usually considered in relation to decay of neutron-star internal or surface fields. Its temperature-independence would also simplify evolutionary calculations such as those of Page et al. For the reasons summarized here, we suggest that the structure of the solid phase of neutron-star matter is not an irrelevant detail. The standard assumption of a homogeneous *bcc* lattice is not adequate and the consequences of an amorphous and *Z*-heterogeneous structure should be included in very many different studies of neutron-star physics.

ACKNOWLEDGMENTS

It is a pleasure to thank Dr J Rikowska Stone for introducing me to the Strutinsky procedure.

REFERENCES

- Ainsworth T. L., Wambach J., Pines D., 1989, *Phys. Lett. B*, 222, 173
- Anderson P. W., Itoh N., 1975, *Nat.*, 256, 25
- Brown E. F., Bildsten L., 1998, *ApJ*, 496, 915
- Chabanat E., Bonche P., Haensel P., Meyer J., Schaeffer R., 1998, *Nucl. Phys. A*, 635, 231
- De Blasio F. V., Lazzari G., 1998, *Nucl. Phys. A*, 633, 391
- De Blasio F. V., 2000, *A&A*, 353, 1129
- Douchin F., Haensel P., 2000, *Phys. Lett. B*, 485, 107
- Douchin F., Haensel P., 2001, *A&A*, 380, 151
- Flowers E., Ruderman M. A., 1977, *ApJ*, 215, 302
- Geppert U., Rheinhardt M., 2002, *A&A*, 392, 1015
- Gnedin O. Y., Yakovlev D. G., Potekhin A. Y., 2001, *MNRAS*, 324, 755
- Haensel P., Pichon B., 1994, *A&A*, 283, 313
- Heiselberg H., Hjorth-Jensen M., 2000, *Phys. Rep.*, 328, 237
- Hollerbach R., Rüdiger G., 2002, *MNRAS*, 337, 216
- Itoh N., Kohyama Y., 1993, *ApJ*, 404, 268
- Jog C. J., Smith R. A., 1982, *ApJ*, 253, 839
- Jones P. B., 1988, *MNRAS*, 233, 875
- Jones P. B., 1999a, *Phys. Rev. Lett.*, 83, 3589
- Jones P. B., 1999b, *MNRAS*, 306, 327
- Jones P. B., 2001, *MNRAS*, 321, 167 (Paper I)
- Jones P. B., 2002, *MNRAS*, 335, 733
- Jones P. B., 2003, *ApJ*, 595, 342
- Kaminker A. D., Yakovlev D. G., Gnedin O. Y., 2002, *A&A*, 383, 1076
- Lattimer J. M., Pethick C. J., Ravenhall D. G., Lamb D. Q., 1985, *Nucl. Phys. A*, 432, 646
- Lorenz C. P., Ravenhall D. G., Pethick C. J., 1993, *Phys. Rev. Lett.*, 70, 379
- Mochizuki Y. S., Oyamatsu K., Izuyama T., 1997, *ApJ*, 489, 848
- Møller P., Nix J. R., Kratz K. -L., 1997, *Atomic Data and Nuclear Data Tables*, 66, 131
- Negele J. W., Vautherin G., 1973, *Nucl. Phys. A*, 207, 298
- Oyamatsu K., 1993, *Nucl. Phys. A*, 561, 431
- Page D., Geppert U., Zannias T., 2000, *A&A*, 360, 1052
- Pethick C. J., Ravenhall D. G., 1995, *Ann. Rev. Nucl. Part. Sci.*, 45, 429
- Pethick C. J., Sahrting M., 1995, *ApJ*, 453, L29
- Potekhin A. Y., 1999, *A&A*, 351, 787
- Potekhin A. Y., Chabrier G., Yakovlev D. G., 1997, *A&A*, 323, 415
- Potekhin A. Y., Yakovlev D. G., 2001, *A&A*, 374, 213
- Rickayzen G., 1965, *Theory of Superconductivity*, John Wiley (Interscience), New York
- Ring P., Schuck P., 1980, *The Nuclear Many-Body Problem*, p. 83, Springer-Verlag, New York
- Ruderman M. A., 1976, *ApJ*, 203, 213
- Schatz H., Bildsten L., Cumming A., Wiescher M., 1999, *ApJ*, 524, 1014
- Shen C., Lombardo U., Schuck P., Zuo W., Sandulescu N., 2003, *Phys. Rev. C*, 67, 061302(R)
- Slater J. C., 1963, *Quantum Theory of Molecules and Solids*, Vol. I, McGraw-Hill, New York
- Thompson C., Duncan R. C., 1995, *MNRAS*, 275, 255
- Thompson C., Duncan R. C., 1996, *ApJ*, 473, 322
- Thompson C., Duncan R. C., Woods P. M., Kouveliotou C., Finger F. H., van Paradijs J., 2000, *ApJ*, 543, 340
- Urpin V. A., Yakovlev D. G., 1980, *Sov. Ast.*, 24, 303
- Urpin V. A., Muslimov A. G., 1992, *MNRAS*, 256, 261
- Watanabe G., Iida K., 2003, *Phys. Rev. C*, 68, 045801

This paper has been typeset from a \TeX / \LaTeX file prepared by the author.